Acta Oceanol. Sin., 2020, Vol. 39, No. 3, P. 56–62
https://doi.org/10.1007/s13131-019-1510-7
http://www.hyxb.org.cn
E-mail: hyxbe@263.net

Observation of internal waves with OLCI and SRAL on board Sentinel-3

Xudong Zhang[1, 2], Jie Zhang[1], Junmin Meng[1]*, Chenqing Fan[1], Jing Wang[2]

[1] First Institute of Oceanography, Ministry of Natural Resources, Qingdao 266061, China

[2] College of Information and Engineering, Ocean University of China, Qingdao 266100, China

Received 24 October 2018; accepted 21 November 2018

Abstract

The ocean and land color instrument (OLCI) and synthetic aperture radar altimeter (SRAL) installed aboard the Sentinel-3 satellite have been in orbit for operational uses. In this study, data collected from Sentinel-3 are used to investigate internal waves in the South China Sea. An internal wave is detected using an OLCI image with a resolution of 300 m, and an analysis was performed with a quasi-synchronous moderate-resolution imaging spectroradiometer (MODIS) image. The opposite characteristics of OLCI and MODIS images of the same internal wave are explained by the critical angle in brightness reversals. The unique observational geometry of the OLCI image and its influence on observations of internal waves are discussed. The distribution of σ_0 and sea surface height anomalies (SSHAs) induced by internal waves are studied using SRAL records. The σ_0 records of SRAL occasionally show less sensitivity to the modulation of internal waves, which may be attributed to the observational geometry, while SSHAs show obvious variations. The synchronous pairing of OLCI images and SRAL records are analyzed to extract the three-dimensional sea surface signatures induced by internal waves. The analysis demonstrates that the profile of SSHAs in the surface shows an opposite phase to the profiles of internal waves in the ocean. The opposite phase relationship, observed in the remote sensing view, is also confirmed with a laboratory experiment.

Key words: internal wave, Sentinel-3, SAR mode altimeter, OLCI

Citation: Zhang Xudong, Zhang Jie, Meng Junmin, Fan Chenqing, Wang Jing. 2020. Observation of internal waves with OLCI and SRAL on board Sentinel-3. Acta Oceanologica Sinica, 39(3): 56–62, doi: 10.1007/s13131-019-1510-7

1 Introduction

The remote sensing has proven to be a powerful technique to detect internal waves (Jackson, 2007; Kozlov et al., 2014; Alford et al., 2015; Guo et al., 2016). The properties of internal waves, such as their generation mechanisms (Bai et al., 2014) and refraction or reflection patterns (Bai et al., 2017), have been investigated in a broader view with satellite images. Synthetic aperture radar (SAR) and optical remote sensing tools, such as the moderate-resolution imaging spectroradiometer (MODIS) and the medium-resolution imaging spectrometer (MERIS), have been used widely for the observation of internal waves. Parameters such as the amplitude (Zheng et al., 2001; Zhang et al., 2016; Pan et al., 2018) and propagation speed (Liu et al., 2014) of internal waves can be extracted from satellite images. By using the advantages of the wide swath of optical remote sensing images, the spatial and temporal distribution of internal waves have been investigated (Jackson, 2007). Their different appearances on optical remote sensing images have also been studied (Melsheimer and Keong, 2001; Jackson and Alpers, 2010). Developments in remote sensing techniques and the proliferation of satellite images have improved our understanding of internal waves. Satellite images only record the internal wave-induced sea surface signatures in a two-dimensional view. The surface elevation induced by an internal wave is small compared with the internal wave amplitude and cannot easily be observed using satellite images, but recorded measurements demonstrate that the surface elevation induced by an internal wave could be observed clearly from a ship (Ramp et al., 2004; Alford et al., 2010; Bai et al., 2013).

The altimeter is an important remote sensor for the measurement of ocean topography. Traditional altimeters, such as Topex/Poseidon, ERS, Envisat, and Jason series, have been used in the measurements of ocean topography (Zaouche et al., 2010) and internal tides (Zhao, 2016) as well as other parameters (Morrow and Le Traon, 2012; Jiang et al., 2016). Altimeters receives echoes from nadir point. Approximately 5% of Ku band observational data have presented high radar return cross sections, which are usually called Sigma0 blooms (Tran et al., 2002). Not all Sigma0 blooms could be accounted for low wind speed, some may represent returns from surfaces where centimeter-scale waves are suppressed (Mitchum et al., 2004) due to the presence of surface films that effectively dampen short-scale wind waves. The propagation of internal waves modulate the gravity capillary waves on the surface and hence changes the sea surface roughness (Alpers, 1985; da Silva et al., 1998). The modulation of internal waves can also be observed by the altimeter, which opens up the possibility that altimetry could be another data source for the study of internal waves. The application of Jason-2 high sampling data for the observation of internal waves has been re-

Foundation item: The National Key R&D Program of China under contract No. 2016YFC1401005; the National Youth Natural Science Foundation of China under contract Nos 41906157 and 61501130; the National Natural Science Foundation of China under contract No. 61471136; the Global Change and Air-Sea Interaction Program of China under contract No. GASI-02-SCS-YGST2-04.
*Corresponding author, E-mail: mengjm@fio.org.cn

ported recently (da Silva and Cerqueira, 2016; Magalhães and da Silva, 2017; Zhang et al., 2018). Parameters such as significant wave height and sigma0 were extracted from the altimeter dataset, and obvious responses were found in the areas where internal waves were detected using quasi-synchronous satellite images, although the time gap between the altimetry data and the satellite images made the synergy study of internal waves more difficult.

Two new instruments, which are carried on the newly launched Sentinel-3A with unique features compared with previous sensors. The ocean and land color instrument (OLCI) boarded on Sentinel-3 has a spatial resolution of approximately 300 m and a unique observational geometry with westerly tilted cameras. The new generation SAR altimeter (SRAL) boarded on Sentinel-3 is the first instrument that provides 100% SAR altimetry data. The along-track resolution of the SAR altimeter has been increased to approximately 300 m. Case studies have been made of observations of Andaman Sea internal waves using SAR mode altimetry (Santos-Ferreira et al., 2018).

In this study, the performance and unique observational geometry of OLCI images are analyzed together with SRAL observations for the study on internal waves. Perfect synchronous pairs of OLCI images and SRAL records are analyzed for observations of internal waves in the South China Sea (SCS). A three-dimensional description of sea surface signatures induced by internal waves is obtained with the synchronous pairs. Section 2 of this article presents the data. In Section 3, the quasi-synchronous observations of internal waves with OLCI and MODIS images are presented and analyzed. In Section 4, the perfect synchronous observations of internal waves with OLCI images and SRAL records from Sentinel-3A are presented. In Section 5, the conclusions are summarized.

2 Data

The MODIS mounted on the Terra and Aqua has 36 bands, the swath is 2 330 km, and the spatial resolutions of MODIS images are 250 m, 500 m, and 1 000 m. MODIS images have a high temporal resolution that can observe the same area twice per day. In this article, L1b MODIS images with a spatial resolution of 250 m are used for the observation of internal waves.

Sentinel-3A was launched on 16 February 2016 as a successor to the ERS-1, ERS-2 and ENVISAT satellites. To continue the coverage of the ERS/ENVISAT missions, Sentinel-3 has almost the same orbital parameters as ENVISAT. The orbital altitude of Sentinel-3 is 815 km, which increases the revisit time from 35 d to 27 d. Sentinel-3 carries four instruments: OLCI, SRAL, the Sea and Land Surface Temperature Radiometer and the Microwave Radiometer. Data from the OLCI and SRAL instruments are used in this article. The design of OLCI is inherited from ENVISAT MERIS with a full spatial resolution of 300 m and a swath of 1 270 km (Bonekamp et al., 2016). The OLCI has 5 cameras with 21 distinct bands. To mitigate sun-glint contamination, the cameras are tilted in a westerly direction by 12.6°, which allows new insights into internal waves. The dual-frequency (Ku and C bands) SRAL can provide 100% SAR mode measurements in the open seas. The application of SAR mode increases the along-track resolution to approximately 300 m. The OLCI images and SRAL records can provide perfect synchronous observation of internal waves.

3 Quasi-synchronous observation of internal waves with OLCI and MODIS images

Internal waves propagating to the northwest in the SCS were detected in the MODIS image acquired at 2:50 on August 7, 2017 and OLCI image acquired at 2:30 on August 7, 2017, as shown in Fig. 1. Three profiles (red lines in Fig. 1) across the wavefront were chosen to extract the peak to trough distances (the distance between the brightest and darkest points) of internal waves for both images. The peak to trough distances measured from the OLCI image are 1 009.2 m, 1 441.6 m and 947.6 m while measurements from the MODIS image are 1 213.5 m, 1 636.9 m and 1 224.7 m, respectively. The measurements obtained from the two satellite images are close and discrepancies can be explained by the 20 min time interval and different spatial resolutions, which validates the use of OLCI images for the observation of internal waves.

The insert map in Fig. 1 shows the profiles across the wavefronts at the locations indicated by the red symbols on the two images. The profiles of internal waves show opposite imaging characteristics on OLCI and MODIS images. The internal wave appears as dark-bright bands on the OLCI image and bright-dark bands on the MODIS image. According to the specular reflection mechanism, the dark band indicates an increased sea surface roughness and the bright band indicates a decreased sea surface roughness. For depression internal waves, the sea surface rough-

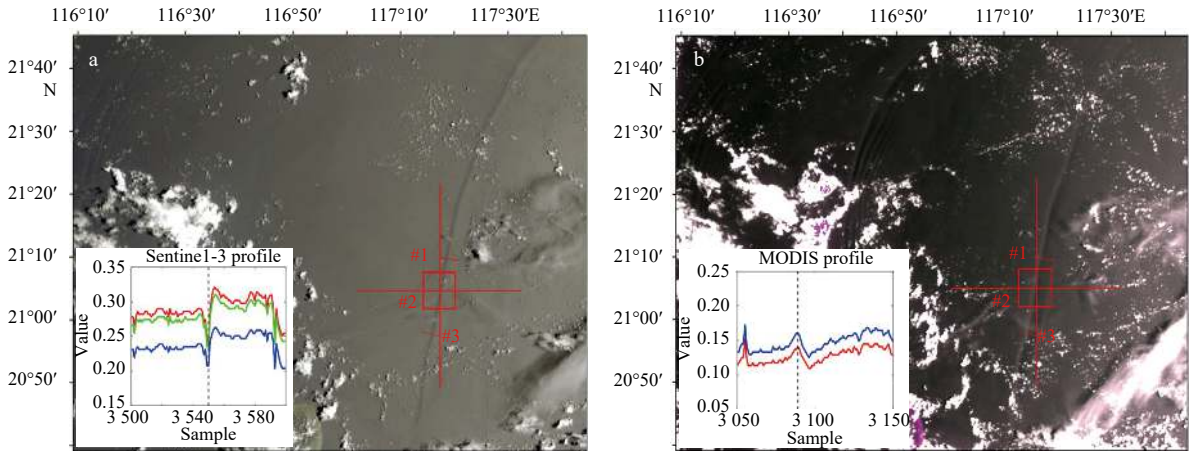

Fig. 1. Observation of internal waves in the SCS using OLCI and MODIS images: a. an OLCI image acquired at 2:30 on August 7, 2017; b. a MODIS image acquired at 2:50 on August 7, 2017. The insert graphs show the profiles of internal waves taken from two images. The red symbols on the images indicate the locations where the profiles are plotted.

ness will increase on the leading edge and decrease on the trailing edge. Sea stratification is not favorable for the generation of elevation internal waves because the observation is in deep water and the upper layer is thinner than the bottom layer. The opposite imaging characteristics from different regions of the same image has been explained by the critical angle in the brightness reversals (Jackson, 2007; Jackson and Alpers, 2010). The opposite imaging characteristics of the two images in the same location are analyzed below.

The normalized sun glint radiance received by the sensor can be expressed by:

$$N_n = \frac{\rho(\omega)}{4} p\left(\theta, \theta_0, \Phi, \sigma^2\right) \frac{\left(1+\tan^2\beta\right)^2}{\cos\theta},$$

where $\rho(\omega)$ is the Fresnel reflection coefficient, $p\left(\theta, \theta_0, \Phi, \sigma^2\right)$ is the probability density function (PDF) of the wave slope, β is the surface tilt and θ is the incidence angle of the sensor. The PDF and surface tilt can be expressed by:

$$p\left(\theta, \theta_0, \Phi, \sigma^2\right) = \frac{1}{\pi\sigma^2}\exp\left(\frac{-\tan^2\beta}{\sigma^2}\right),$$

and

$$\tan^2\beta = \frac{\sin^2\theta_0 + \sin^2\theta + 2\sin\theta_0\sin\theta\cos\Phi}{(\cos\theta_0 + \cos\theta)},$$

where θ_0 is the solar zenith angle, Φ is the relative azimuth angle and σ^2 is the sea surface roughness variance. When exploring the critical sensing viewing angle, a symmetric PDF is introduced. The sea surface roughness is independent of wind direction as expressed by Cox and Munk (1954):

$$\sigma^2 = 0.003 + 0.005\ 12U,$$

where U is the wind speed. Different values for sea surface roughness are produced by different wind speeds. In this study, wind speeds of 2 m/s, 6 m/s and 10 m/s are adopted to simulate different sea surface roughness. The parameters, such as the solar zenith angle, are extracted from the metadata and auxiliary data of OLCI and MODIS images. Values for normalized radiance are calculated and used to construct radiance profiles across the fronts of the internal wave along the zonal direction, as shown in Fig. 2 and Fig. 3.

The red lines in Fig. 2 indicate profiles with less sea surface roughness and blue lines indicate profiles with greater sea surface roughness. Intersections of different profiles mean that a brightness reversal may occur. As shown in Fig. 2, only one brightness reversal occurs on the OLCI image around 116°E, while two brightness reversals occur on the MODIS image around longitude 117°E and 122°E. The wind speeds here are chosen randomly in order to show different values for sea surface roughness as analogous to the sea surface roughness variations caused by internal waves.

The opposite imaging characteristics of internal waves on the OLCI and MODIS images as shown in Fig. 1 can now be explained. As shown in Fig. 3, the internal wave on the OLCI image is located in the dark-bright region in Fig. 2. The lesser surface roughness will produce higher radiance. On the other hand, the internal waves on the MODIS image are located in the bright-dark region where higher surface roughness produces higher radiance. A depression internal wave propagating in the ocean will result in an increase of sea surface roughness at the leading edge. The sea surface roughness at the trailing edge of an internal wave will decrease. Therefore, the internal wave shows dark-bright bands in the OLCI image while bright-dark bands are observed on the MODIS image.

As shown in Fig. 2, the peak of radiance profiles on the OLCI image is very close to the right side of the image when compared with those on the MODIS image. This is due to the westerly tilted cameras as described in Section 2, which make it easier to interpret internal waves on OLCI images. In addition, the mitigation of sun glint by westerly tilted cameras will also result in less received light which may cause additional difficulties in the observation of internal waves, especially for small scale internal waves.

4 Synchronous observation of internal waves with OLCI images and SRAL records

Detection of internal waves with quasi-synchronous data from traditional altimeter and satellite images has been explored (da Silva and Cerqueira, 2016; Magalhães and da Silva, 2017; Zhang et al., 2018). The OLCI and SRAL on Sentinel-3A provide perfect synchronous observations of internal waves. The synchronous pairing of OLCI images and SRAL records will be

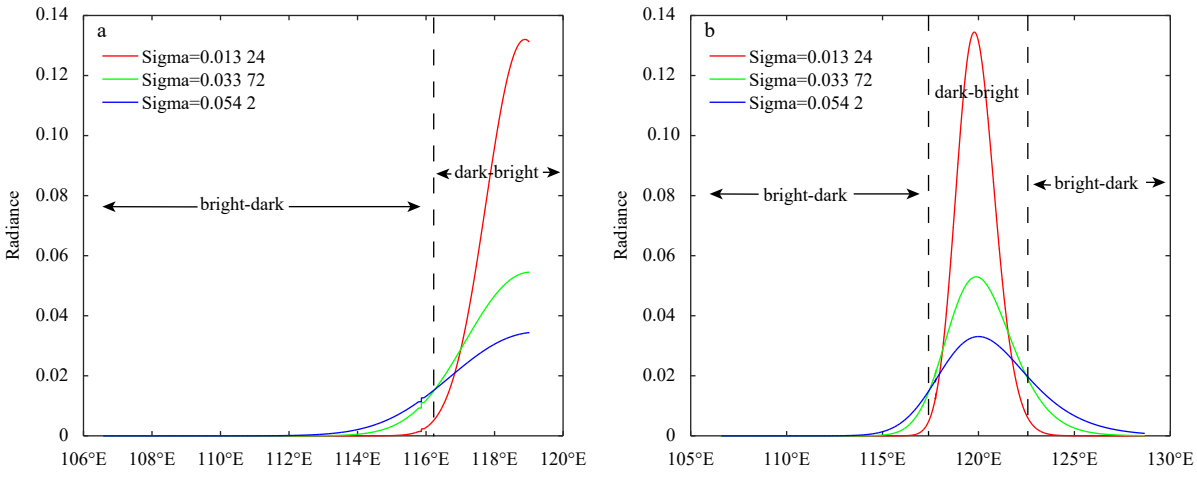

Fig. 2. Profiles of normalized radiance for the OLCI image (a) and MODIS image (b).

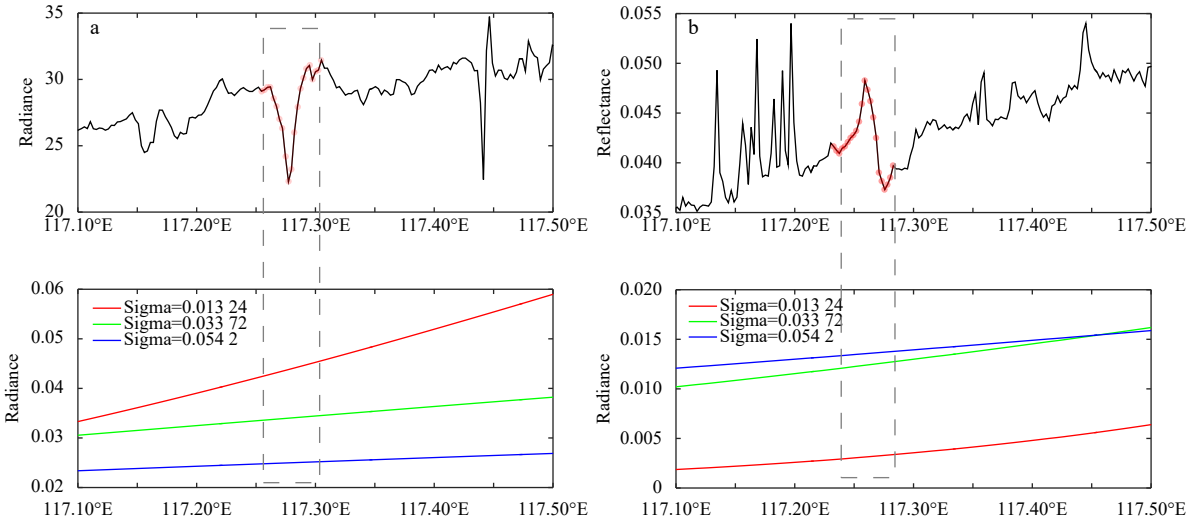

Fig. 3. Profiles of measured (top) and calculated (bottom) radiance for OLCI (a) and MODIS (b) images. The gray dashed boxes indicate the position of internal waves. Red shaded data in the gray dashed boxes indicate profiles of internal waves.

presented next and the sea surface signatures induced by internal waves will be discussed in this section.

Internal waves propagating to the northwest were observed on the OLCI image in the SCS on April 29, 2017. Meanwhile, the wavefronts of internal wave intersect with the ground tracks of SRAL at around 21.87°N, as shown in Fig. 4. Almost no clouds were observed in the OLCI image during the observation, which practically excludes the rain or liquid water contamination of altimeter received echoes. The geophysical parameters were extracted from the L2 products of SRAL. As shown in previous work of internal wave detection using Jason-2, the distribution of σ_0 and off-nadir angle is altered with the existence of internal waves (Magalhães and da Silva, 2017). Their work showed that the sea surface height anomaly (SSHA) induced by internal waves was as large as 1 m.

As shown in Fig. 4, contrary to the performance of traditional altimeters (Magalhães and da Silva, 2017), the distribution of σ_0 in the Ku and C bands shows little variation from the influence of internal waves. This finding may be accounted for the observational geometry between the SRAL and the internal waves. The footprint of the SRAL is oblique to the internal wave crests which causes averaging of positive and negative contributions to the radar backscatter, averaging out the signature (Santos-Ferreira et al., 2018). However, as shown in Fig. 5, another case in the Celebes Sea shows obvious variations of σ_0 in the Ku band and SSHA as well. Obvious variations can also be found in cases presented by Santos-Ferreira et al. (2018) in the Andaman Sea and the tropical North Atlantic. For cases in the SCS, the ground tracks of altimeters are almost parallel to the wavefront of internal waves in the Dongsha Atoll, while for cases in the Celebes Sea and the Andaman Sea the ground tracks of altimeters are almost perpendicular to the wavefront. This may explain the different responses of radar backscatter.

The distribution of σ_0 shows little variation for cases in the SCS while the distribution of SSHA shows an obvious variation of approximately 0.5 m. Several reports in the literature suggest that the propagation of internal waves will show surface solitons in the sea surface, and these traveling solitons have been observed

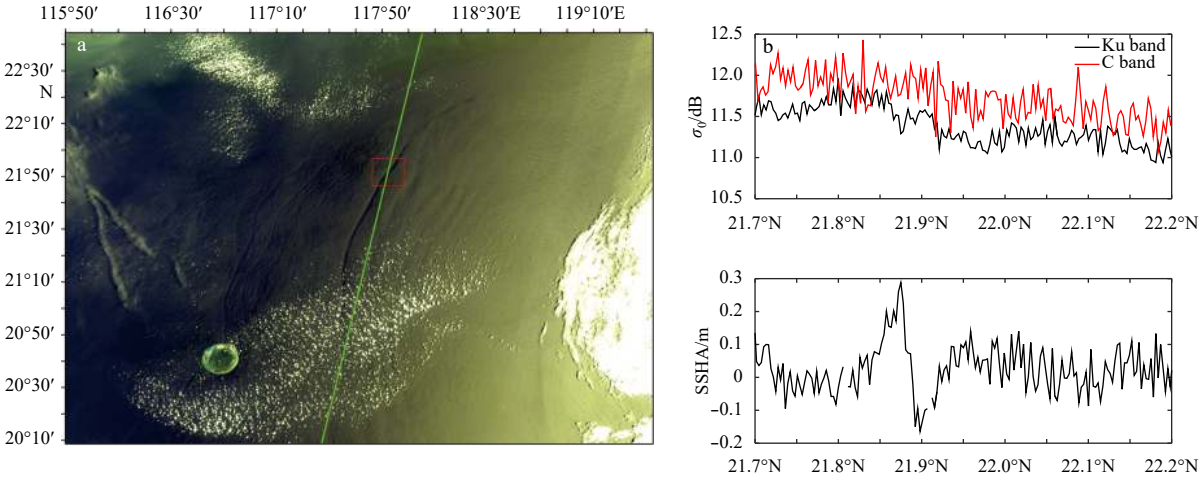

Fig. 4. Synchronous observation of internal waves with the OLCI image and SRAL records acquired on April 29, 2017 (a) and the spatial distribution of σ_0 and SSHA (b). The green line indicates the ground tracks of Sentinel-3A and the red box indicates the locations of intersections.

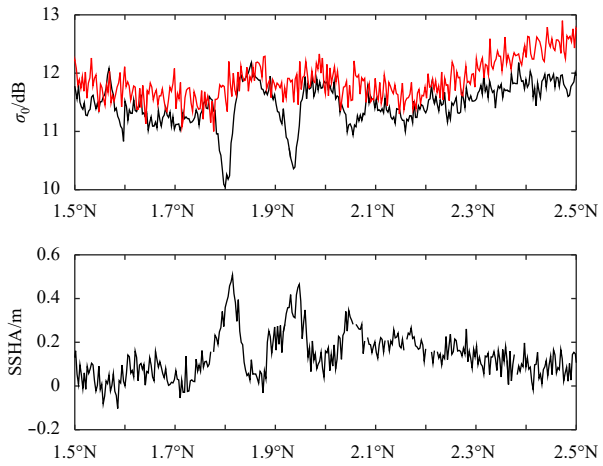

Fig. 5. The spatial distribution of σ_0 and SSHA obtained from SRAL records in the Celebes Sea on March 28, 2017.

by field experiments (Bai et al., 2013; Osborne and Burch, 1980). OLCI images and SRAL records provide profiles of internal waves and induced sea surface signatures. To investigate the relationship between the vertical displacement of internal waves in the ocean and the surface elevation of the ocean, the profiles of internal waves on the OLCI image and the distribution of SSHA from the synchronous SRAL records are shown in Fig. 6.

As shown in Fig. 6, the locations of peak SSHAs correspond to the center of dark and bright bands extracted from the OLCI image. The propagation of internal waves will induce convergence and divergence on the sea surface, which results in bright-dark or dark-bright bands on the OLCI image. A conceptual graph that reveals the relation between the profile of internal waves and sea surface signatures is shown in Fig. 7. The center of dark and bright bands corresponds to the maximum vertical displacement of a depression internal wave in the ocean. Therefore, the maximum elevation on the surface corresponds to the maximum downward displacement of internal wave profiles. Wave-induced surface elevation is opposite in phase to the internal wave profile (Gill, 1982).

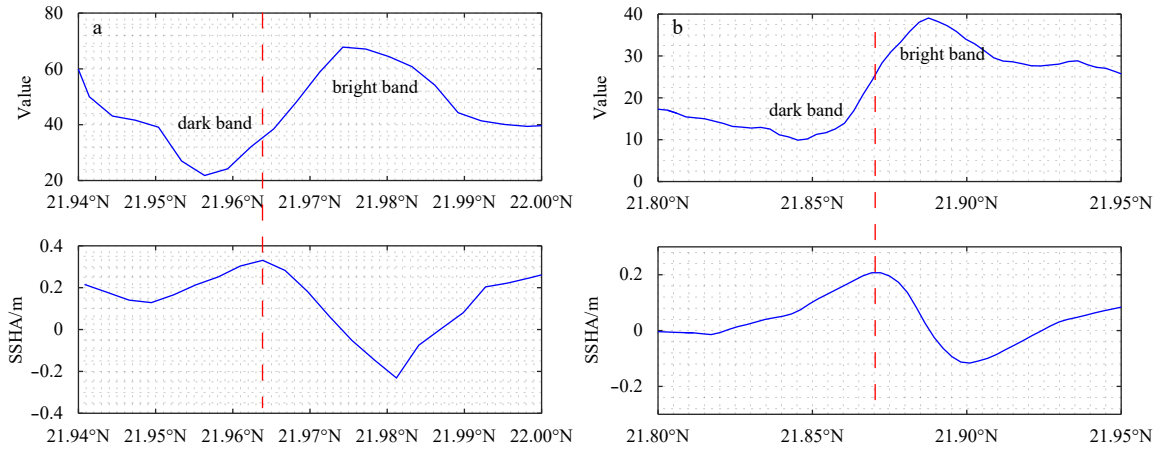

Fig. 6. The profile of internal waves extracted from OLCI images and the corresponding spatial distribution of SSHA acquired on April 29 (a) and September 11 (b), 2017. The red dashed line indicates the peak of SSHA.

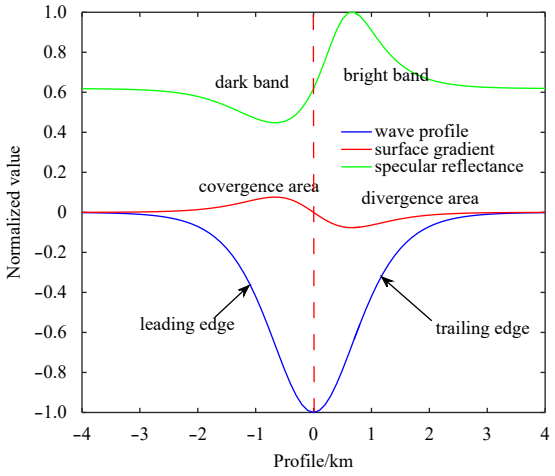

Fig. 7. Conceptual overview of the imaging process of internal waves on optical remote sensing images. The red dashed line indicates the location of the maximum vertical displacement of the internal wave profile.

To confirm the results from the remote sensing records, a laboratory experiment was conducted in a tank that is 15 m long, 0.35 m wide and 0.7 m high to verify the opposite phase relationship in the remote sensing view. The water in the experimental tank is two-layer stratified with a total height of 0.44 m. The depth of the upper layer is 0.1 m, and the depth of the lower layer is 0.34 m. Two CCD cameras are used (one on the top and one on the side of the tank) to record the experiment with a sampling frequency of 50 Hz. The side camera observes the profile of internal waves and the surface variations during the experiment. The height of the side camera is the same as the pycnocline. The experimental apparatus and pictures taken by the side camera are presented in Fig. 8.

To have a better view of internal wave profiles, the time series along a fixed location is extracted as shown in Fig. 9. A total of 1 500 pictures are recorded during the experiment which corresponds to an observation time of 30 s. The bottom figure in Fig. 9 corresponds to the red line in Fig. 8b. In the top figure in Fig. 9, the surface elevation is enlarged, making it obvious. The opposite-phase relation between the profiles of internal wave and the surface elevation is demonstrated in Fig. 9 and is consistent with the remote sensing results. Hence, the results from both the re-

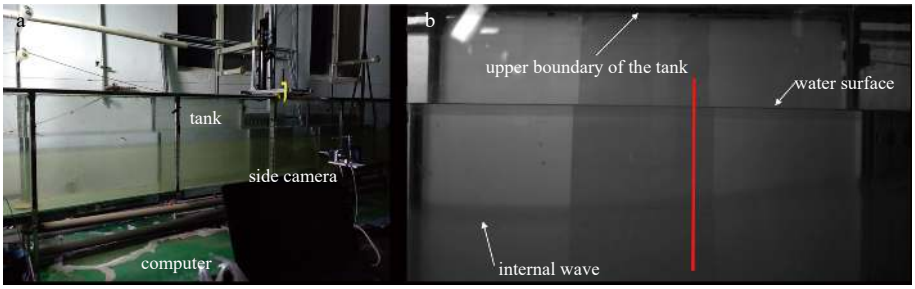

Fig. 8. The experimental apparatus (a) and pictures taken by the side camera (b). The red line in the bottom figure shows the location of the extracted time series.

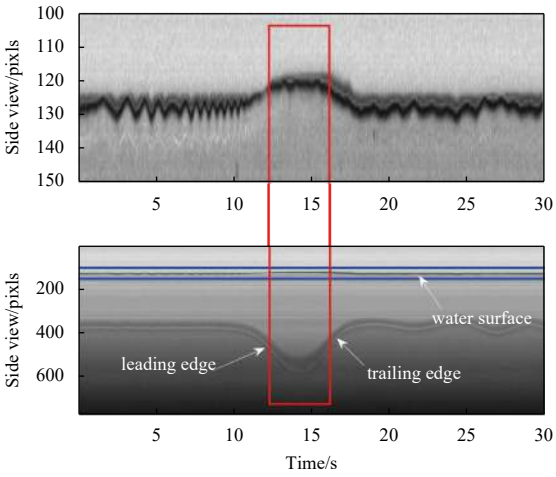

Fig. 9. The time series extracted from pictures taken by the side camera is shown in the bottom figure. The blue box indicates the location of the water surface. The top figure is an enlarged view.

mote sensing and the laboratory experiment reveal that the peak of the surface profiles corresponds to the maximum displacement of internal waves in the ocean in accordance with theory (Gill, 1982). The results are made possible by the availability of perfect synchronous pairs from OLCI images and SRAL records, which provide the opportunity to detect internal waves with SSHA data.

5 Conclusions

Two new instruments are carried on the newly launched Sentinel-3A with unique features compared with previous sensors. The utility of OLCI images for observing internal waves is analyzed using a quasi-synchronous MODIS image. The results show that internal waves can be easily observed on OLCI images with a spatial resolution of 300 m. The opposite imaging characteristics of internal waves on OLCI images and MODIS images with a 20 min interval is analyzed. The different imaging characteristics are explained by the critical angle in brightness reversals. This analysis also shows that the westerly tilted cameras on the OLCI could make the interpretation of internal waves easier because only one brightness reversal occurs. On the other hand, less light will be received by the cameras which will make it more difficult to observe internal waves, especially for small scale internal waves.

With the perfect synchronous observation of internal waves based on the OLCI and SRAL, the extracted geophysical parameters of SRAL are analyzed. For cases in the SCS, the sigma0 of SRAL records shows less sensitivity. The reason for the insensitivity may be attributed to the observational geometry between the ground tracks of SRAL and the propagating direction of internal waves. The clear internal wave signatures observed in the distribution of SSHAs demonstrate that the SSHAs could serve as a possible indicator for the detection of internal waves using SRAL records. The sea surface signatures of internal waves are investigated with synchronous OLCI images and SRAL records. The analysis demonstrates that the surface elevation induced by internal waves shows an opposite phase to the profiles of internal waves in the ocean. The results from a designed laboratory experiment also confirm this relationship. The three-dimensional sea surface signatures induced by internal waves are investigated owing to the synchronous observation of OLCI and SRAL boarded on Sentinel-3. This study indicates that altimetry data are important for the study of internal waves. The launch of Sentinel-3 may bring new insights to the investigation of internal waves.

Acknowledgements

The MODIS image is provided by NASA-the Level-1 and Atmosphere Archive & distribution System (LAADS) distributed Active Archive Center (DAAC). The Sentinel-3 dataset is provided by Copernicus Online Data Access (https://coda.eumetsat.int).

References

Alford M H, Lien R C, Simmons H, et al. 2010. Speed and evolution of nonlinear internal waves transiting the South China Sea. Journal of Physical Oceanography, 40(6): 1338–1355, doi: 10.1175/2010JPO4388.1

Alford M H, Peacock T, MacKinnon J A, et al. 2015. The formation and fate of internal waves in the South China Sea. Nature, 521(7550): 65–69, doi: 10.1038/nature14399

Alpers W. 1985. Theory of radar imaging of internal waves. Nature, 314(6008): 245–247, doi: 10.1038/314245a0

Bai Xiaolin, Li Xiaofeng, Lamb K G, et al. 2017. Internal Solitary Wave Reflection Near Dongsha Atoll, the South China Sea. Journal of Geophysical Research: Oceans, 122(10): 7978–7991, doi: 10.1002/2017JC012880

Bai Xiaolin, Liu Zhiyu, Li Xiaofeng, et al. 2014. Generation sites of internal solitary waves in the southern Taiwan Strait revealed by MODIS true-colour image observations. International Journal of Remote Sensing, 35(11–12): 4086–4098, doi: 10.1080/01431161.2014.916453

Bai Xiaolin, Liu Zhiyu, Li Xiaofeng, et al. 2013. Observations of high-frequency internal waves in the Southern Taiwan Strait. Journal of Coastal Research, 29(6): 1413–1419, doi: 10.2112/JCOASTRES-D-12-00141.1

Bonekamp H, Montagner F, Santacesaria V, et al. 2016. Core operational Sentinel-3 marine data product services as part of the Copernicus Space Component. Ocean Science, 12(3): 787–795, doi: 10.5194/os-12-787-2016

Cox C, Munk W. 1954. Measurement of the roughness of the sea surface from photographs of the sun's glitter. Journal of the Optical Society of America, 44(11): 838–850, doi: 10.1364/JOSA.44.000838

Da Silva J C B, Cerqueira A L F. 2016. A note on radar altimeter signatures of internal solitary waves in the ocean. In: Remote Sensing of the Ocean, Sea Ice, Coastal Waters, and Large Water Regions 2016. Edinburgh, United Kingdom: SPIE

Da Silva J C B, Ermakov S A, Robinson I S, et al. 1998. Role of surface films in ERS SAR signatures of internal waves on the shelf: 1. Short-period internal waves. Journal of Geophysical Research: Oceans, 103(C4): 8009–8031, doi: 10.1029/97JC02725

Gill A E. 1982. Atmosphere-Ocean Dynamics (International Geophysics Series). London: Academic Press

Guo Daquan, Akylas T R, Zhan Peng, et al. 2016. On the generation and evolution of internal solitary waves in the southern Red Sea. Journal of Geophysical Research: Oceans, 121(12): 8566–8584, doi: 10.1002/2016JC012221

Jackson C. 2007. Internal wave detection using the moderate resolution imaging spectroradiometer (MODIS). Journal of Geophysical Research: Oceans, 112(C11): C11012, doi: 10.1029/2007JC004220

Jackson C R, Alpers W. 2010. The role of the critical angle in brightness reversals on sunglint images of the sea surface. Journal of Geophysical Research: Oceans, 115(C9): C09019

Jiang Maofei, Xu Ke, Liu Yalong, et al. 2016. Estimating the sea state bias of Jason-2 altimeter from crossover differences by using a three-dimensional nonparametric model. IEEE Journal of Selected Topics in Applied Earth Observations and Remote Sensing, 9(11): 5023–5043, doi: 10.1109/JSTARS.2016.2557839

Kozlov I, Romanenkov D, Zimin A, et al. 2014. SAR observing large-scale nonlinear internal waves in the White Sea. Remote Sensing of Environment, 147: 99–107, doi: 10.1016/j.rse.2014.02.017

Liu Bingqing, Yang Hong, Zhao Zhongxiang, et al. 2014. Internal solitary wave propagation observed by tandem satellites. Geophysical Research Letters, 41(6): 2077–2085, doi: 10.1002/2014GL059281

Magalhães J M, da Silva J C B. 2017. Satellite altimetry observations of large-scale internal solitary waves. IEEE Geoscience and Remote Sensing Letters, 14(4): 534–538, doi: 10.1109/LGRS.2017.2655621

Melsheimer C, Keong K L. 2001. Sun glitter in SPOT images and the visibility of oceanic phenomena.Singapore: The 22nd Asian Conference on Remote Sensing.

Mitchum G T, Hancock D W III, Hayne G S, et al. 2004. Blooms of σ^0 in the TOPEX radar altimeter data. Journal of Atmospheric and Oceanic Technology, 21(8): 1232–1245, doi: 10.1175/1520-0426(2004)021<1232:BOITTR>2.0.CO;2

Morrow R, Le Traon P Y. 2012. Recent advances in observing mesoscale ocean dynamics with satellite altimetry. Advances in Space Research, 50(8): 1062–1076, doi: 10.1016/j.asr.2011.09.033

Osborne A R, Burch T L. 1980. Internal solitons in the Andaman Sea. Science, 208(4443): 451–460, doi: 10.1126/science.208.4443.451

Pan Xiaoyi, Wang Jing, Zhang Xudong, et al. 2018. A deep-learning model for the amplitude inversion of internal waves based on optical remote-sensing images. International Journal of Remote Sensing, 39(3): 607–618, doi: 10.1080/01431161.2017.1390269

Ramp S R, Tang T Y, Duda T F, et al. 2004. Internal solitons in the northeastern South China Sea. Part I: sources and deep water propagation. IEEE Journal of Oceanic Engineering, 29(4): 1157–1181, doi: 10.1109/JOE.2004.840839

Santos-Ferreira A M, da Silva J C B, Magalhaes J M. 2018. SAR mode altimetry observations of internal solitary waves in the tropical ocean Part 1: Case studies. Remote Sensing, 10(4): 644, doi: 10.3390/rs10040644

Tran N, Hancock D W III, Hayne G S, et al. 2002. Assessment of the cycle-to-cycle noise level of the Geosat Follow-On, TOPEX, and Poseidon altimeters. Journal of Atmospheric and Oceanic Technology, 19(12): 2095–2107, doi: 10.1175/1520-0426(2002)019<2095:AOTCTC>2.0.CO;2

Zaouche G, Perbos J, Lafon T, et al. 2010. OSTM/Jason-2: Assessment of the system performances (ocean surface topography mission: OSTM). Marine Geodesy, 33(S1): 26–52

Zhang Xudong, Wang Jing, Sun Lina, et al. 2016. Study on the amplitude inversion of internal waves at Wenchang area of the South China Sea. Acta Oceanologica Sinica, 35(7): 14–19, doi: 10.1007/s13131-016-0902-1

Zhang Xudong, Zhang Jie, Fan Chenqing, et al. 2018. Observations of internal waves with high sampling data of radar altimetry and MODIS images. International Journal of Remote Sensing, 39(21): 7405–7416, doi: 10.1080/01431161.2018.1470700

Zhao Zhongxiang. 2016. Using CryoSat-2 altimeter data to evaluate M_2 internal tides observed from multisatellite altimetry. Journal of Geophysical Research: Oceans, 121(7): 5164–5180, doi: 10.1002/2016JC011805

Zheng Quanan, Yuan Yeli, Klemas V, et al. 2001. Theoretical expression for an ocean internal soliton synthetic aperture radar image and determination of the soliton characteristic half width. Journal of Geophysical Research: Oceans, 106(C12): 31415–31423, doi: 10.1029/2000JC000726